

Atmospheric
mercury pollution in
Beijing

L. Zhang et al.

Atmospheric mercury concentration and chemical speciation at a rural site in Beijing, China: implication of mercury emission sources

L. Zhang¹, S. X. Wang^{1,2}, L. Wang¹, and J. M. Hao^{1,2}

¹State Key Joint Laboratory of Environmental Simulation and Pollution Control, School of Environment, Tsinghua University, Beijing 100084, China

²State Environmental Protection Key Laboratory of Sources and Control of Air Pollution Complex, Beijing 100084, China

Received: 26 March 2013 – Accepted: 18 April 2013 – Published: 8 May 2013

Correspondence to: S. X. Wang (shxwang@tsinghua.edu.cn)

Published by Copernicus Publications on behalf of the European Geosciences Union.

Title Page

Abstract

Introduction

Conclusions

References

Tables

Figures

◀

▶

◀

▶

Back

Close

Full Screen / Esc

Printer-friendly Version

Interactive Discussion



Abstract

Continuous measurements of atmospheric mercury concentration and speciation play a key role in identifying mercury sources and its behavior in the atmosphere. In this study, speciated atmospheric mercury including gaseous elemental mercury (GEM), reactive gaseous mercury (RGM) and particle-bound mercury (PBM) were continuously measured at Miyun, a rural site in Beijing, China from December 2008 to November 2009. The average GEM, RGM and PBM concentrations were found to be $3.22 \pm 1.74 \text{ ng m}^{-3}$, $10.1 \pm 18.8 \text{ pg m}^{-3}$ and $98.2 \pm 112.7 \text{ pg m}^{-3}$, respectively, about 2–20 times of the background concentration of Northern Hemisphere. The results indicated that atmospheric mercury concentrations in North China were highly affected by anthropogenic emissions. The atmospheric mercury showed obvious seasonal variations with the highest seasonal average GEM concentration in summer (3.48 ng m^{-3}) and the lowest value in winter (2.66 ng m^{-3}). In autumn and winter a diurnal variation of GEM was observed with peak levels in late afternoon till midnight. Most of the high RGM concentration values occurred in the afternoon of all seasons due to the higher oxidation. The PBM concentration was higher in early morning of all seasons because of the atmospheric stratification during nighttime against laminar fluxes during daytime. The ratio of GEM to CO indicates that residential boilers play an important role in the elevation of GEM in winter. The ratio of RGM to O_3 could be an indicator of the contribution of local primary sources. The ratio of PBM to $\text{PM}_{2.5}$ reveals that the air mass from east and southwest to the site in spring and summer carries more atmospheric mercury. The HYSPLIT back-trajectory analysis indicated that the monitoring site is affected by local, regional and interregional sources simultaneously during heavy pollution episodes. The results from the potential source contribution function (PSCF) model indicate that the atmospheric transport predominantly from the northwest contribute to the elevated atmospheric mercury in winter and autumn, while the North China Plain (NCP) Region and the north part of Yangtze River Delta (YRD) Region are the major source areas for mercury pollution in spring and summer.

Atmospheric mercury pollution in Beijing

L. Zhang et al.

Title Page

Abstract

Introduction

Conclusions

References

Tables

Figures



Back

Close

Full Screen / Esc

Printer-friendly Version

Interactive Discussion



1 Introduction

As a global pollutant, atmospheric mercury has been paid to great attention for its long-range transport and toxicity. Atmospheric mercury can be categorized into total gaseous mercury (TGM) and particle-bound mercury (PBM) in physical forms. TGM is further divided into gaseous elemental mercury (GEM) and reactive gaseous mercury (RGM). Schroeder and Munthe (1998) reported that GEM, accounting for over 95% of TGM, has a long residence time in the atmosphere from 0.5 to 2 years. However, based on soil–air exchange fluxes and deposition, Gustin et al. (2008) suggested that the residence time for GEM in the air is on the order of hours to weeks. Atmospheric mercury monitoring is a fundamental approach to understand the atmospheric mercury behavior of one region and is also used to identify the local and regional mercury emission sources coupling with back trajectory models.

According to the existing data, the global background concentration of atmospheric mercury is considered to be in the range of 1.5–1.7 ng m⁻³ in the Northern Hemisphere and 1.1–1.3 ng m⁻³ in the Southern Hemisphere (Fu et al., 2012a; Lindberg et al., 2007). There were plenty of studies conducted in the rural areas in the United States since 2000. Sheu et al. (2002) conducted a one-year study in Stillpond, Maryland and found the annual average GEM, RGM and PBM concentration to be 1.7 ± 0.5 ng m⁻³, 21 ± 22 pg m⁻³ and 42 ± 50 pg m⁻³, respectively. Studies conducted in Pompano Beach, Florida (Malcolm et al., 2003) showed similar results for GEM (1.6–2.0 ng m⁻³) but much lower ranges for both RGM (1.6–4.9 pg/m³) and PBM (0.7–6.3 pg/m³). Lynam and Keeler (2005) reported that the GEM, RGM and PBM concentrations in Dexter, Michigan were respectively 1.49–1.51 ng m⁻³, 2–3 pg m⁻³ and 7–17 pg m³. Study of Gabriel et al. (2005) on Cove Mountain in Tennessee obtained a GEM average as high as 3.2 ng m⁻³ and the RGM and PBM concentrations were 16.4 pg m⁻³ and 9.7 pg m⁻³, respectively. A five-year monitoring performed in Great Mountain Forest, Connecticut (Sigler and Lee, 2006) gave out a GEM range to be 1.4–1.6 ng m⁻³. Similarly the GEM range of 1.3–1.6 ng m⁻³ was found in Salmon Creek

Atmospheric mercury pollution in Beijing

L. Zhang et al.

Title Page

Abstract

Introduction

Conclusions

References

Tables

Figures

◀

▶

◀

▶

Back

Close

Full Screen / Esc

Printer-friendly Version

Interactive Discussion



**Atmospheric
mercury pollution in
Beijing**

L. Zhang et al.

Title Page

Abstract

Introduction

Conclusions

References

Tables

Figures

◀

▶

◀

▶

Back

Close

Full Screen / Esc

Printer-friendly Version

Interactive Discussion



Falls Reservoir, Idaho (Abbott et al., 2007). Valente et al. (2007) reported the GEM, RGM and PBM concentrations to be 1.65 ng m^{-3} , 5 pg m^{-3} and 7 pg m^{-3} respectively in Look Rock, Tennessee. Laurier and Mason (2007) found in Chesapeake Bay Laboratory, Maryland that the GEM and RGM concentrations were $1.7\text{--}1.8 \text{ ng m}^{-3}$ and $6\text{--}13 \text{ pg m}^{-3}$, respectively.

China is one of the largest mercury emission sources in the world (AMAP and UNEP, 2008). However, to date, relatively limited field measurements had been conducted in China to investigate the atmospheric processes of mercury. Most previous studies focused on the urban areas and mining/industrial regions (Fang et al., 2001; Liu et al., 2002; Feng et al., 2004; Wang et al., 2007; Zhu et al., 2012). A few studies were conducted at the mountain sites such as Mt. Waliguan, Mt. Gongga, and Mt. Changbai (Wang et al., 2007; Fu et al., 2008a,b, 2009, 2010a; Zhu et al., 2008; Wan et al., 2009a,b). There is lack of mercury monitoring data in rural area or regional background for typical regions in China such as North China Plain (NCP) Region. Most of these studies only measured atmospheric mercury and did not simultaneously observe the concentrations of other air pollutants such as fine particles ($\text{PM}_{2.5}$), carbon monoxide (CO), and ozone (O_3), which could help to identify the emission sources and explain the atmospheric behavior of mercury.

In this study, we measured the GEM, RGM and PBM as well as $\text{PM}_{2.5}$, CO, and O_3 at a rural site in North China for a whole year. We analyzed the temporal variation of mercury species and summarized the correlation between mercury and other air pollutants to investigate the factors affecting its behaviors in the region. Furthermore, based on the NOAA HYSPLIT model and the potential source contribution function (PSCF) model, the potential mercury sources and emission regions were analyzed, which helped to improve the understanding of atmospheric mercury outflow from China.

2 Methodology

2.1 Monitoring site description

The mercury monitoring station (40° 28' 51" N, 116° 46' 30" E, 220 m a.s.l.) in this study was located in Miyun County, about 100 km northeast to the Beijing urban area (see Fig. 1). The Miyun County is famous for its Miyun Reservoir, one of the biggest reservoirs in North China, supplying Beijing residents with fresh water. The surrounding areas within 20 km from the site are largely rural, without large point source in any directions. Miyun has temperate continental monsoon climate, controlled by cold Siberian–Mongolian high pressure in winter with northwest wind dominated and impacted by Continental low and Pacific high pressure in summer with southeast wind dominated. The mercury emission sources in Beijing urban area are considered as the local sources for the monitoring station, which is shown in Fig. 1. The mercury emissions in the North China Plain (NCP) Region, including Beijing, Tianjin, the south part of Hebei, the north part of Henan and the west part of Shandong are regarded as regional sources for the site. The mercury emissions outside NCP region are all regarded as the interregional sources for this site.

2.2 Atmospheric mercury monitoring

Automatic atomic fluorescence mercury monitoring system, composed of TekranTM 2537B, 1130 and 1135, was employed in this study for measurements of GEM, RGM and PBM (Landis et al., 2002). Although Gustin et al. (2013) and Lyman et al. (2013) addressed that concentrations of reactive mercury (RGM + PBM) measured by the TekranTM system may be underestimated due to the release of mercury halides from KCl denuders in the presence of ozone, the TekranTM system is the most accurate instrument system so far and widely used for observation of speciated mercury in the ambient air.

Atmospheric
mercury pollution in
Beijing

L. Zhang et al.

Title Page

Abstract

Introduction

Conclusions

References

Tables

Figures

◀

▶

◀

▶

Back

Close

Full Screen / Esc

Printer-friendly Version

Interactive Discussion



The analytical module 2537B uses cold vapor atomic fluorescence spectroscopy (CVAFS) with the detection limit of 0.1 ng m^{-3} at the sampling flow rate of 1.0 L min^{-1} . GEM is continuously measured by 2537B every five minutes. The denuder coated with KCl in 1130 and the quartz filter in 1135 are designed to capture RGM and PBM respectively. Since there is an impactor at the bottom of 1130 to remove particles larger than $2.5 \mu\text{m}$, PBM in this study is actually referred to $\text{PBM}_{2.5}$, i.e. the mercury on $\text{PM}_{2.5}$. The sampling inlet is 1.5 m above the instrument platform. Both units are configured to collect 1 h samples at a flow rate of 10 L min^{-1} , resulting in a detection limit of 0.5 pg m^{-3} for RGM and PBM. After 1 h sampling, the quartz filter and the denuder turn to mercury desorption mode in succession at the temperature of 800°C and 500°C respectively. 1130 and 1135 systems are flushed with Hg-free air during the next 1 h period, and RGM and PBM are sequentially thermodesorbed and analyzed. The denuder was re-coated every two weeks in case of passivation. The 2537B analyzer was calibrated automatically every 25 h using the internal mercury permeation source inside the instrument, and the internal permeation source was calibrated every six months with manual injection of mercury by a syringe from an external mercury source (module 2505). Two zeros and two spans were performed in each calibration for gold trap A and B, respectively. The error between gold trap A and gold trap B was limited to $\pm 10\%$. The meteorological parameters such as wind speed, wind direction, air temperature, and relative humidity were measured using Vantage Pro2TM weather station (Davis Instruments). CO , O_3 and $\text{PM}_{2.5}$ concentrations were also monitored using Thermo ScientificTM Model48i-TLE CO Analyzer, Model49i O_3 Analyzer and TEOM1405, respectively. The instrument details are discussed in Wang et al. (2008). All the data were hourly averaged for this study.

2.3 Meteorological data and backward trajectory calculation

The HYSPLIT (Hybrid Single-Particle Lagrangian Integrated Trajectory) model developed by the National Oceanic and Atmospheric Administration (NOAA) is a complete

Atmospheric mercury pollution in Beijing

L. Zhang et al.

Title Page

Abstract

Introduction

Conclusions

References

Tables

Figures

◀

▶

◀

▶

Back

Close

Full Screen / Esc

Printer-friendly Version

Interactive Discussion



system for computing simple air parcel trajectories to complex dispersion and deposition simulations. In this study, Global Data Assimilation System (GDAS) data with one-degree latitude-longitude horizontal resolution was used for source identification. Back trajectories were calculated for typical pollution events. The total run time was 48 h which can cover China, Mongolia and east Russia. The start time was 4:00 a.m. and restarted every 6 h. The trajectory arrival height (a.g.l) was set as 500 m to represent the boundary layer where pollutants are usually well mixed.

The potential source contribution function (PSCF) is a useful statistical tool based on the HYSPLIT model to identify source areas for pollutants with a relatively long life-time such as elemental mercury and CO (Xu and Akhtar, 2010). The PSCF values for grid cells in a study domain are calculated by counting the trajectory segment endpoints that terminate within each cell. The number of endpoints that fall in the ij th cell is designated n_{ij} . The number of endpoints for the same cell having arrival times at the sampling site corresponding to GEM concentrations higher than a specific criterion is defined to be m_{ij} . The PSCF value for the ij th cell is then defined as:

$$\text{PSCF}_{ij} = \frac{m_{ij}}{n_{ij}} W_{ij} \quad (1)$$

Where W_{ij} is an empirical weight to reduce the effects of grid cells with small n_{ij} values. In this study, W_{ij} is defined in following formula in which Avg is the mean n_{ij} of all grid cells with n_{ij} greater than zero.

$$W_{ij} = \begin{cases} 1.0 & n_{ij} > 2 \cdot \text{Avg} \\ 0.7 & \text{Avg} < n_{ij} \leq 2 \cdot \text{Avg} \\ 0.42 & 0.5 \cdot \text{Avg} < n_{ij} \leq \text{Avg} \\ 0.17 & n_{ij} \leq 0.5 \cdot \text{Avg} \end{cases} \quad (2)$$

The PSCF value indicates the probability of a grid cell through which pollution events occurs. In this study, the domain which covers Chinese mainland (73.5° E–134.5° E,

18.5° N–53.5° N), is divided into 8450 grid cells with 0.5° × 0.5° resolution. Three-day back trajectories are generated hourly from 1 January to 11 November in 2009 by TrajStat (Wang et al., 2009), a software including HYSPLIT for trajectory calculation with trajectory statistics modules. PSCF maps are plotted using ARCGIS version 9.3.

3 Characteristics of speciated mercury concentration

3.1 General characteristics of speciated mercury in atmosphere

Speciated mercury concentration data with a one-year period from December 2008 to November 2009 was obtained by the TekranTM mercury monitoring system. The hourly averaged GEM, RGM and PBM concentrations are shown in Fig. 2. The average GEM concentration in Miyun Station is $3.22 \pm 1.74 \text{ ng m}^{-3}$, while those of RGM and PBM are $10.1 \pm 18.8 \text{ pg m}^{-3}$ and $98.2 \pm 112.7 \text{ pg m}^{-3}$, respectively (see Table 1). GEM accounts for over 95 % of the total mercury concentration. The average total mercury concentration is 3.3 ng m^{-3} , about 2 times of the background concentration of Northern Hemisphere (Lindberg et al., 2007). Table 2 listed the TGM, PBM and RGM concentrations from existing literatures. The TGM concentration of this rural site in Beijing is higher than that of most remote sites, while lower than that of most urban sites. The PBM concentration of this rural site in Beijing is higher than that of all remote sites, while lower than that of all urban sites. The median value of GEM is 9 % lower than the mean value. The interval of 1st and 3rd quartiles lies in the range of 1.81–4.12 ng m^{-3} . However, the mean values of RGM and PBM are much higher than the median values respectively. The mean/median ratios for RGM and PBM are 2.0 and 1.7, respectively. Comparing the mean values of RGM and PBM with the results from the monitoring sites in rural areas in the USA (Valente et al., 2007; Gabriel et al., 2005; Lynam and Keeler, 2005; Malcolm et al., 2003), the RGM concentration of the Miyun site is more or less at the same level as those of American sites. However, the PBM concentration of the Miyun site is much higher than those of American sites, which reflects the

Title Page

Abstract

Introduction

Conclusions

References

Tables

Figures



Back

Close

Full Screen / Esc

Printer-friendly Version

Interactive Discussion



severe PM pollution problem in North China. There are several extreme peaks in the observation of the three mercury species. Most of the GEM and PBM peaks match well with the highest air pollution index (API) values in Beijing urban area (shown in Fig. 2), indicating the influence of heavy pollution episodes in Beijing, especially for the period of 3 to 8 November 2009.

3.2 Seasonal variation of speciated mercury concentration

The seasonal variation of GEM, RGM and PBM is shown in Fig. 3. December–February is considered to be winter, March–May to be spring, June–August to be summer, and September–November to be autumn. The highest seasonal average GEM concentration occurs in summer (3.48 ng m^{-3}), while winter has the lowest value (2.66 ng m^{-3}). However, the case of PBM concentration is the opposite. The PBM concentration is higher in winter and lower in summer. The variation range of GEM is relatively larger in spring and autumn than that in winter and summer. The variation range of PBM is smaller in summer than other seasons. From winter to autumn, the RGM concentration gets higher, and the variation range of it becomes larger. RGM is either directly released by anthropogenic sources or formed by the photochemical processes with the oxidation of GEM. The seasonal variation of RGM indicates that the photochemical oxidation processes were more active in summer and autumn than in winter and spring. The heavy pollution episodes in autumn were longer and heavier than those in other seasons, which led to the highest seasonal average RGM concentration in autumn. The dominant wind directions for all the four seasons are northeast. Nevertheless, the second dominant wind directions for spring and summer are east and southwest. Therefore the monitoring site is mainly influenced by the northern areas in China, as well as the east and southwest directions in spring and summer.

Atmospheric mercury pollution in Beijing

L. Zhang et al.

Title Page

Abstract

Introduction

Conclusions

References

Tables

Figures

◀

▶

◀

▶

Back

Close

Full Screen / Esc

Printer-friendly Version

Interactive Discussion



3.3 Diurnal variation of speciated mercury concentration

In spring and summer, no significant diurnal variation is found for GEM, as is shown in Fig. 4a. The GEM concentration from late afternoon till midnight (16:00–2:00) is higher than the rest of the day in autumn and winter. For the RGM concentration in Fig. 4b, most of the high values occur in the afternoon (13:00–15:00) of all four seasons. This is probably related to the intensity of solar radiation. With higher intensity of solar radiation in the afternoon, more GEM is oxidized to RGM. However, the RGM concentration peak for autumn is higher than that for summer, which is due to the heavy pollution episodes in autumn. The PBM concentration, shown in Fig. 4c, is higher in the early morning (01:00–06:00) of all four seasons, which is probably caused by atmospheric stratification during nighttime against laminar fluxes during daytime, driven by wind secular periodicity. The daily variation of RGM and PBM reflects the formation and removal mechanisms of these two short lifetime mercury species. Photochemical reaction is the main process for RGM formation, while deposition and adsorption to particles are the two main processes for RGM removal. Adsorption of GEM and RGM to particles is the main process for PBM formation, while rain and dispersion are important processes for PBM removal.

3.4 Correlations between mercury species and meteorological factors

Among all meteorological factors, wind direction has the most significant impact on the concentrations of different mercury species. Figure 5 shows the GEM, RGM and PBM concentrations and wind direction frequency in different wind directions. Southwest wind was the dominant wind direction in the monitoring period with both high frequency and high wind speed. The high average GEM and PBM concentrations from the southwest direction suggest that the southwest wind brought the most atmospheric mercury pollution to the monitoring site. The influence of wind direction on RGM is not as remarkable as that on GEM and PBM, because RGM is also highly related to other meteorological factors, such as solar radiation. Temperature and relative humidity also

Title Page

Abstract

Introduction

Conclusions

References

Tables

Figures

◀

▶

◀

▶

Back

Close

Full Screen / Esc

Printer-friendly Version

Interactive Discussion



has considerable influence on different mercury species with seasonal variations, as shown in Table 3. RGM concentration has higher dependence on temperature in spring and summer than in autumn and winter, indicating higher RGM formation from photochemical reactions in spring and summer. No correlation was found between temperature and GEM or PBM concentration. The correlations between GEM concentration and relative humidity are notable with little seasonal variation, which is possibly due to the same pattern of diurnal variation of GEM and relative humidity, i.e. lower at daytime and higher at night. RGM concentration is positively related to relative humidity in winter while negatively in summer. It reveals that moisture in the atmosphere could both scavenge RGM by wet deposition under higher temperature in summer and enhance RGM formation by strengthening the oxidation process under lower temperature in winter. PBM concentration has considerable correlation with relative humidity, higher in winter than other seasons. This implies that moisture probably contributes to the formation of PBM, and this influence is amplified under lower temperature.

4 Mercury source attribution via multi-pollutant correlations

4.1 Source type identification

GEM concentration has a significant correlation with CO concentration due to their homology. Industrial coal combustion, domestic coal combustion, cement production and iron and steel production are the dominant anthropogenic emission sources for both pollutants (Wu et al., 2006; Wang et al., 2005). Except for these four types of sources, vehicles are another type of dominant sources for CO, while power plants and non-ferrous metal smelters are another two types of dominant sources for GEM. GEM also has significant natural background, which CO does not. Figure 6 shows the relationship between GEM concentration and CO concentration by season.

The slope of the trend line represents the ratio of GEM emission to CO emission (Hg/CO ratio). For the monitoring station in this study in North China, the GEM con-

Title Page

Abstract

Introduction

Conclusions

References

Tables

Figures

◀

▶

◀

▶

Back

Close

Full Screen / Esc

Printer-friendly Version

Interactive Discussion



Atmospheric mercury pollution in Beijing

L. Zhang et al.

Title Page

Abstract

Introduction

Conclusions

References

Tables

Figures



Back

Close

Full Screen / Esc

Printer-friendly Version

Interactive Discussion

centration is mainly influenced by coal combustion, including power plants, industrial boilers and residential boilers, while the CO concentration is mainly influenced by coal combustion and vehicles. Non-ferrous metal smelters, the second largest anthropogenic source of mercury, are mainly located in the southern part of China, and thus have little influence on the GEM concentration of this station. Based on existing studies (Wang et al., 2005; Wu et al., 2006), the Hg/CO ratio for power plants is larger than that for industrial and residential boilers. In 2001, the Hg/CO ratios for power plants, industrial boilers and residential boilers were 25.2, 2.9 and 0.4, respectively (Wang et al., 2005; Wu et al., 2006). Incomplete combustion such as residential coal combustion and biomass burning could lead to a lower Hg/CO ratio. The Hg/CO ratio for vehicles is almost zero. Weiss-Penzias et al. (2007) reported Hg/CO ratios of 5.7, 1.5 and 0.8 for Asian long-range transport (ALRT), Pacific Northwest US biomass burning (BB PNW) and Alaska biomass burning (BB Alaska), respectively. As shown in Fig. 6, The Hg/CO ratio for winter, spring, summer and autumn are 1.50, 3.04, 2.43 and 3.24, respectively. One of the main causes for the lower Hg/CO ratio in winter could be that the activity level of residential coal combustion is higher in winter. The Hg/CO ratios in Fig. 6 indicate that residential boilers play an important role in mercury pollution in winter.

The intercept of the trend line mainly reflects the intensity of natural background of GEM. The intercept for summer is higher than those for other seasons because the natural mercury emissions are higher in summer in terms of higher atmospheric temperature. However, the intercept for autumn is lower than that for winter, which is probably due to the heavy GEM pollution episodes. Most of the GEM concentration values higher than 10 ng m^{-3} were from 5 and 6 November 2009, resulting in the counterclockwise rotation of the trend line and thus the decrease of the intercept.

The correlation coefficients of the trend lines for winter, spring, summer and autumn are 0.89, 0.71, 0.74 and 0.79 respectively. The correlation coefficient implies the contribution rate of homological emission sources (e.g. industrial coal combustion, residential coal combustion, cement production and iron and steel production) to GEM concentra-

tion, which fits quite well with the fact that the correlation coefficient for winter is much higher than that for other seasons, because the activity level of coal combustion in North China is higher in winter for heating supply.

4.2 Impacts of local primary sources

O_3 is a secondary pollutant and originates from photochemical process and thus highly depends on the intensity of solar radiation. RGM is formed either directly from local emission sources (i.e. primary RGM) or from the photochemical oxidation of GEM (i.e. secondary RGM). Considering the shorter residence time of both RGM and O_3 compared with GEM, the primary RGM emitted directly from emission sources can be considered as the direct influence of the local sources.

The comparison of O_3 and RGM concentrations in different seasons is shown in Fig. 7. In winter, both the RGM and O_3 were at low level due to low intensity of radiation, while both concentrations were high in summer. The coherence of the variation of RGM and O_3 was high in spring and summer while low in autumn and winter. This indicates that the monitoring site is more directly influenced by local sources in autumn and winter, while the secondary RGM is more important in spring and summer.

After sequencing the RGM/ O_3 ratio, the moving correlation coefficients of every 100 pairs of O_3 -RGM were calculated. Figure 8 shows the relationship between the moving average RGM/ O_3 ratio and the moving O_3 -RGM correlation coefficient. It reveals that the O_3 -RGM correlation coefficient decreases when the RGM/ O_3 ratio increases in the range of $0.05\text{--}2\text{pg m}^{-3}\text{ ppb}^{-1}$. This implies that the ratio of RGM to O_3 could be an indicator of local primary sources. Higher RGM/ O_3 ratio suggests higher influence from local primary sources. The exceptions outside the common RGM/ O_3 ratio range were mainly because the RGM or O_3 concentrations were fairly low ($\text{RGM} < 1\text{ pg m}^{-3}$, $\text{O}_3 < 2\text{ ppb}$). The peak values of the RGM/ O_3 ratio occurred in the period from 3 to 8 November 2009. The back trajectory analysis indicated that this period was mainly influenced by local emission sources, as shown in Sect. 5.1.

Atmospheric mercury pollution in Beijing

L. Zhang et al.

Title Page

Abstract

Introduction

Conclusions

References

Tables

Figures

◀

▶

◀

▶

Back

Close

Full Screen / Esc

Printer-friendly Version

Interactive Discussion



4.3 Source direction identification

Relationships between PBM and $PM_{2.5}$ have obvious seasonal variations, as shown in Fig. 9. The slope of the trend line means the ratio of PBM to $PM_{2.5}$. The ratios for winter, spring, summer and autumn are 2.66×10^{-6} , 3.06×10^{-6} , 3.35×10^{-6} and 2.56×10^{-6} , respectively. Wind direction is a key factor for the variations. Based on the meteorological data, the dominant wind directions for all the four seasons are northeast wind. However, the subdominant wind direction for spring and summer are east wind and southwest wind. The particles from the north are mainly sand storms from Inner Mongolia, a natural source of particles whose mercury content is low. The particles from the south are mainly from North China Region including Beijing urban area. Most of these particles with high mercury content are emitted from anthropogenic sources, such as coal-fired boilers. Therefore, the slope of the trend line for the relationship between $PM_{2.5}$ and PBM could reveal the mercury source direction. The ratios reveal that the air mass from east and southwest to the site in spring and summer carries more atmospheric mercury.

5 Mercury source attribution via HYSPLIT modeling

5.1 Identification of mercury sources during heavy pollution episodes

HYSPLIT is a modeling tool to visualize the long-range transport of air mass so as to track the spatial sources of certain pollutants. HYSPLIT modeling was performed for three heavy pollution episodes respectively in spring, summer and autumn, 4–6 May (episode I), 12–14 August (episode II) and 5–7 November (episode III), 2009 with a run-time of 48 h, shown as Fig. 10. The average GEM, RGM and PBM concentrations for these three episodes are listed in Table 1. The dominant mercury species for the first episode in spring were GEM and PBM, while that for the second episode in summer was RGM. The concentrations of all the three mercury species were significantly high

Atmospheric mercury pollution in Beijing

L. Zhang et al.

[Title Page](#)[Abstract](#)[Introduction](#)[Conclusions](#)[References](#)[Tables](#)[Figures](#)[◀](#)[▶](#)[◀](#)[▶](#)[Back](#)[Close](#)[Full Screen / Esc](#)[Printer-friendly Version](#)[Interactive Discussion](#)

which has reached the north of YRD Region. The year-round statistics indicate that mercury emission in NCP is the most important contributor of mercury pollution in Miyun site. However, it has to be noted that HYSPLIT model has its limitation and the results could be interfered by the “local signal”.

6 Conclusions

The one-year speciated mercury observation in Miyun from December 2008 to November 2009 indicated that the overall average GEM, RGM and PBM concentrations are $3.22 \pm 1.74 \text{ ng m}^{-3}$, $10.1 \pm 18.8 \text{ pg m}^{-3}$ and $98.2 \pm 112.7 \text{ pg m}^{-3}$, respectively. The seasonal average GEM concentration is higher in summer and lower in winter. The PBM concentration, on the contrary, is higher in winter and lower in summer. RGM, formed by the photochemical processes, has higher concentration and wider range in autumn. No significant daily variation is found for GEM in spring and summer, while in autumn and winter the GEM concentration from late afternoon till midnight is higher than the rest of the day. Most of the high RGM concentration values occur in the afternoon due to the high intensity of solar radiation. The PBM concentration is higher in the early morning of all four seasons, which is probably related to atmospheric stratification during nighttime against laminar fluxes during daytime, driven by wind secular periodicity.

GEM concentration has a significant correlation with CO concentration due to their homology. The slope of the trend line represents the ratio of GEM emission to CO emission, which indicates that residential boilers play an important role in the mercury pollution in winter. The intercept of the trend line reflects the intensity of natural background of GEM. The correlation coefficient of GEM and the CO concentration implies the contribution rate of coal combustion to GEM. The ratio of RGM to O_3 could be an indicator of local primary sources. Moreover, the ratio of PBM to $\text{PM}_{2.5}$ indicates that the air mass from east and southwest to the site in spring and summer carries more atmospheric mercury.

Atmospheric mercury pollution in Beijing

L. Zhang et al.

Title Page

Abstract

Introduction

Conclusions

References

Tables

Figures

◀

▶

◀

▶

Back

Close

Full Screen / Esc

Printer-friendly Version

Interactive Discussion



Atmospheric mercury pollution in Beijing

L. Zhang et al.

Title Page

Abstract

Introduction

Conclusions

References

Tables

Figures



Back

Close

Full Screen / Esc

Printer-friendly Version

Interactive Discussion



From the analysis of heavy pollution episodes using the HYSPLIT model, the monitoring site is simultaneously affected by local, regional and interregional sources, and the most heavily polluted episode is more impacted by the local sources. According to the PSCF statistics based on HYSPLIT model, most of the mercury comes from the remote west and north area to Beijing, including the Loess Plateau and Outer Mongolia in autumn and winter. However, the major sources of mercury in spring and summer are located in the south and east area to Beijing. Mercury emissions from NCP Region to the north part of YRD Region play a more important role in spring and summer than that in autumn and winter.

Acknowledgements. This work was sponsored by Natural Science Foundation of China (No. 20 937 002), Major State Basic Research Development Program of China (973 Program) (No. 2013CB430001) and MEP's Special Funds for Research on Public Welfares (No. 201209015). We would like to thank Nicola Pirrone for his help on the establishment of Miyun mercury monitoring station and Jerry Lin for his valuable suggestions on this paper.

References

Abbott, M., Lin, C. J., Martian, P., and Einerson, J.: Atmospheric Mercury Near Salmon Falls Creek Reservoir in Southern Idaho, INL/EXT-06-12048, Idaho Department of Environmental Quality, Boise, Idaho, 2007.

Arctic Monitoring and Assessment Programme (AMAP), and United Nations Environment Programme (UNEP): Technical Background Report to the Global Atmospheric Mercury Assessment, Geneva, Switzerland, 2008.

Ci, Z. J., Zhang, X. S., Wang, Z. W., and Niu, Z. C.: Atmospheric gaseous elemental mercury (GEM) over a coastal/rural site downwind of East China: temporal variation and long-range transport, *Atmos. Environ.*, 45, 2480–2487, 2011a.

Ci, Z. J., Zhang, X. S., Wang, Z. W., Niu, Z. C., Diao, X. Y., and Wang, S. W.: Distribution and air-sea exchange of mercury (Hg) in the Yellow Sea, *Atmos. Chem. Phys.*, 11, 2881–2892, doi:10.5194/acp-11-2881-2011, 2011b.

Fang, F. M., Wang, Q. C., Liu, R. H., Ma, Z. W., and Hao, Q. J.: Atmospheric particulate mercury in Changchun City, China, *Atmos. Environ.*, 35, 4265–4272, 2001.

**Atmospheric
mercury pollution in
Beijing**

L. Zhang et al.

Title Page

Abstract

Introduction

Conclusions

References

Tables

Figures

◀

▶

◀

▶

Back

Close

Full Screen / Esc

Printer-friendly Version

Interactive Discussion



Fang, F. M., Wang, Q. C., and Li, J. F.: Urban environmental mercury in Changchun, a metropolitan city in northeastern China: source, cycle, and fate, *Sci. Total. Environ.*, 330, 159–170, 2004.

Feng, X. B., Shang, L. H., Wang, S. F., Tang, S. L., and Zheng, W.: Temporal variation of total gaseous mercury in the air of Guiyang, China, *J. Geophys. Res.*, 109, 3303, D03303, doi:10.1029/2003JD004159, 2004.

Friedli, H. R., Arellano Jr., A. F., Geng, F., Cai, C., and Pan, L.: Measurements of atmospheric mercury in Shanghai during September 2009, *Atmos. Chem. Phys.*, 11, 3781–3788, doi:10.5194/acp-11-3781-2011, 2011.

Fu, X. W., Feng, X. B., Zhu, W. Z., Wang, S. F., and Lu, J. L.: Total gaseous mercury concentrations in ambient air in the eastern slope of Mt. Gongga, south-eastern fringe of the Tibetan plateau, China, *Atmos. Environ.*, 42, 970–979, 2008a.

Fu, X. W., Feng, X. B., Zhu, W. Z., Zheng, W., Wang, S. F., and Lu, J. Y.: Total particulate and reactive gaseous mercury in ambient air on the eastern slope of the Mt. Gongga area, China, *Appl. Geochem.*, 23, 408–418, 2008b.

Fu, X. W., Feng, X. B., Wang, S. F., Rothenberg, S., Shang, L. H., Li, Z. G., and Qiu, G. L.: Temporal and spatial distributions of total gaseous mercury concentrations in ambient air in a mountainous area in southwestern China: implications for industrial and domestic mercury emissions in remote areas in China, *Sci. Total. Environ.*, 407, 2306–2314, 2009.

Fu, X. W., Feng, X., Dong, Z. Q., Yin, R. S., Wang, J. X., Yang, Z. R., and Zhang, H.: Atmospheric gaseous elemental mercury (GEM) concentrations and mercury depositions at a high-altitude mountain peak in south China, *Atmos. Chem. Phys.*, 10, 2425–2437, doi:10.5194/acp-10-2425-2010, 2010a.

Fu, X. W., Feng, X. B., Zhang, G., Xu, W. H., Li, X. D., Yao, H., Liang, P., Li, J., Sommar, J., Yin, R. S., and Liu, N.: Mercury in the marine boundary layer and seawater of the South China Sea: concentrations, sea/air flux, and implication for land outflow, *J. Geophys. Res.*, 115, D06303, doi:10.1029/2009JD012958, 2010b.

Fu, X. W., Feng, X. B., Qiu, G. L., Shang, L. H., and Zhang, H.: Speciated atmospheric mercury and its potential source in Guiyang, China, *Atmos. Environ.*, 45, 4205–4212, 2011.

Fu, X. W., Feng, X. B., Sommar, J., and Wang, S. F.: A review of studies on atmospheric mercury in China, *Sci. Total. Environ.*, 421–422, 73–81, 2012a.

**Atmospheric
mercury pollution in
Beijing**

L. Zhang et al.

[Title Page](#)[Abstract](#)[Introduction](#)[Conclusions](#)[References](#)[Tables](#)[Figures](#)[◀](#)[▶](#)[◀](#)[▶](#)[Back](#)[Close](#)[Full Screen / Esc](#)[Printer-friendly Version](#)[Interactive Discussion](#)

Fu, X. W., Feng, X., Shang, L. H., Wang, S. F., and Zhang, H.: Two years of measurements of atmospheric total gaseous mercury (TGM) at a remote site in Mt. Changbai area, northeastern China, *Atmos. Chem. Phys.*, 12, 4215–4226, doi:10.5194/acp-12-4215-2012, 2012b.

Fu, X. W., Feng, X., Liang, P., Deliger, Zhang, H., Ji, J., and Liu, P.: Temporal trend and sources of speciated atmospheric mercury at Waliguan GAW station, northwestern China, *Atmos. Chem. Phys.*, 12, 1951–1964, doi:10.5194/acp-12-1951-2012, 2012c.

Gabriel, M. C., Williamson, D. G., Brooks, S., and Lindberg, S.: Atmospheric speciation of mercury in two contrasting Southeastern US airsheds, *Atmos. Environ.*, 39, 4947–4958, 2005.

Gustin, M. S., Lindberg, S. E., and Weisberg, P. J.: An update on the natural sources and sinks of atmospheric mercury, *Appl. Geochem.*, 23, 482–493, 2008.

Gustin, M. S., Huang, J. Y., Miller, M. B., Peterson, C., Jaffe, D. A., Ambrose, J., Finley, B. D., Lyman, S. N., Call, K., Talbot, R., Feddersen, D., Mao, H. T., and Lindberg, S. E.: Do we understand what the mercury speciation instruments are actually measuring? results of RAMIX, *Environ. Sci. Technol.*, doi:10.1021/es3039104, in press, 2013.

Landis, M. S., Stevens, R. K., Schaedlich, F., and Prestbo, E. M.: Development and characterization of an annular denuder methodology for the measurement of divalent inorganic reactive gaseous mercury in ambient air, *Environ. Sci. Technol.*, 36, 3000–3009, 2002.

Laurier, F. and Mason, R.: Mercury concentration and speciation in the coastal and open ocean boundary layer, *J. Geophys. Res.*, 112, D06302, doi:10.1029/2006JD007320, 2007.

Li, Z., Xia, C. H., Wang, X. M., Xia, Y. R., and Xie, Z. Q.: Total gaseous mercury in Pearl River Delta region, China during 2008 winter period, *Atmos. Environ.*, 45, 834–838, 2011.

Lindberg, S., Bullock, R., Ebinghaus, R., Engstrom, D., Feng, X. B., Fitzgerald, W., Pirrone, N., Prestbo, E., and Seigneur, C.: A synthesis of progress and uncertainties in attributing the sources of mercury in deposition, *Ambio*, 36, 19–32, 2007.

Liu, S. L., Nadim, F., Perkins, C., Carley, R. J., Hoag, G. E., Lin, Y. H., and Chen, L. T.: Atmospheric mercury monitoring survey in Beijing, China, *Chemos.*, 48, 97–107, 2002.

Lynam, M. and Keeler, G. J.: Artifacts associated with the measurement of particulate mercury in an urban environment: the influence of elevated ozone concentrations, *Atmos. Environ.*, 39, 3081–3088, 2005.

Malcolm, E. G., Keeler, G. J., and Landis, M. S.: The effects of the coastal environment on the atmospheric mercury cycle, *J. Geophys. Res.*, 108, D04357, doi:10.1029/2002JD003084, 2003.

**Atmospheric
mercury pollution in
Beijing**

L. Zhang et al.

Title Page

Abstract

Introduction

Conclusions

References

Tables

Figures

◀

▶

◀

▶

Back

Close

Full Screen / Esc

Printer-friendly Version

Interactive Discussion



Nguyen, D. L., Kim, J. Y., Shim, S. G., and Zhang, X. S.: Ground and shipboard measurements of atmospheric gaseous elemental mercury over the Yellow Sea region during 2007–2008, *Atmos. Environ.*, 45, 253–260, 2011.

Schroeder, W. H. and Munthe, J.: Atmospheric mercury: an overview, *Atmos. Environ.*, 32, 809–822, 1998.

Sheu, G. R., Mason, R. P., and Lawson, N. M.: Speciation and distribution of atmospheric mercury over the northern Chesapeake Bay, *ACS Symp. Ser.*, 806, 223–242, 2002.

Sigler, J. M. and Lee, X.: Recent trends in anthropogenic mercury emission in the northeast United States, *J. Geophys. Res.*, 111, D14316, doi:10.1029/2005JD006814, 2006.

Sprovieri, F., Pirrone, N., Ebinghaus, R., Kock, H., and Dommergue, A.: A review of worldwide atmospheric mercury measurements, *Atmos. Chem. Phys.*, 10, 8245–8265, doi:10.5194/acp-10-8245-2010, 2010.

Valente, R. J., Shea, C., Lynn Humes, K., and Tanner, R. L.: Atmospheric mercury in the Great Smoky Mountains compared to regional and global levels, *Atmos. Environ.*, 41, 1861–1873, 2007.

Wan, Q., Feng, X. B., Lu, J. L., Zheng, W., Song, X. J., Han, S. J., and Xu, H.: Atmospheric mercury in Changbai Mountain area, northeastern China I: the seasonal distribution pattern of total gaseous mercury and its potential sources, *Environ. Res.*, 109, 201–206, 2009a.

Wan, Q., Feng, X. B., Lu, J., Zheng, W., Song, X. J., Li, P., Han, S. J. and Xu, H.: Atmospheric mercury in Changbai Mountain area, northeastern China II: the distribution of reactive gaseous mercury and particulate mercury and mercury deposition fluxes, *Environ. Res.*, 109, 721–727, 2009b.

Wang, L. T., Zhang, Q., Hao, J. M., and He, K. B.: Anthropogenic CO emission inventory of Mainland China, *Acta. Scientiae. Circumstantiae.*, 25, 1580–1585, 2005. (in Chinese)

Wang, Z. W., Chen, Z. S., Duan, N., and Zhang, X. S.: Gaseous elemental mercury concentration in atmosphere at urban and remote sites in China, *J. Environ. Sci.*, 19, 176–180, 2007.

Wang, Y., McElroy, M. B., Munger, J. W., Hao, J., Ma, H., Nielsen, C. P., and Chen, Y.: Variations of O₃ and CO in summertime at a rural site near Beijing, *Atmos. Chem. Phys.*, 8, 6355–6363, doi:10.5194/acp-8-6355-2008, 2008.

Wang, Y. Q., Zhang, X. Y., and Draxler, R.: TrajStat: GIS-based software that uses various trajectory statistical analysis methods to identify potential sources from long-term air pollution measurement data, *Environ. Modell. Softw.*, 24, 938–939, 2009.

Atmospheric mercury pollution in Beijing

L. Zhang et al.

Title Page

Abstract

Introduction

Conclusions

References

Tables

Figures

◀

▶

◀

▶

Back

Close

Full Screen / Esc

Printer-friendly Version

Interactive Discussion



Table 1. Statistics of the overall monitoring data and averages in heavy pollution periods for the GEM, RGM and PBM at Miyun, Beijing.

		GEM (ngm ⁻³)	RGM (pgm ⁻³)	PBM (pgm ⁻³)
Statistics	Mean value	3.22	10.06	98.19
	Standard deviation	1.74	18.83	112.72
	Minimum	0.39	0.12	0.49
	1st quartile	1.81	2.59	21.78
	Median (2nd quartile)	2.94	5.02	57.31
	3rd quartile	4.12	10.77	134.48
	Maximum	14.83	301.20	1090.24
Heavy pollution episodes	I: 4–6 May, 2009	4.42	4.31	178.37
	II: 12–14 Aug, 2009	3.43	10.92	50.38
	III: 5–7 Nov, 2009	9.69	82.55	373.04

Atmospheric mercury pollution in Beijing

L. Zhang et al.

Table 3. Correlation coefficients between mercury species and meteorological factors in different seasons.

Correlation	Winter	Spring	Summer	Autumn
GEM – temperature	0.21	0.35	−0.06	0.03
RGM – temperature	0.06	0.45	0.46	−0.01
PBM – temperature	0.07	−0.05	−0.20	−0.13
GEM – relative humidity	0.47	0.46	0.48	0.48
RGM – relative humidity	0.40	−0.04	−0.42	0.04
PBM – relative humidity	0.51	0.44	0.31	0.41

[Title Page](#)
[Abstract](#)
[Introduction](#)
[Conclusions](#)
[References](#)
[Tables](#)
[Figures](#)
[Back](#)
[Close](#)
[Full Screen / Esc](#)
[Printer-friendly Version](#)
[Interactive Discussion](#)


Atmospheric mercury pollution in Beijing

L. Zhang et al.

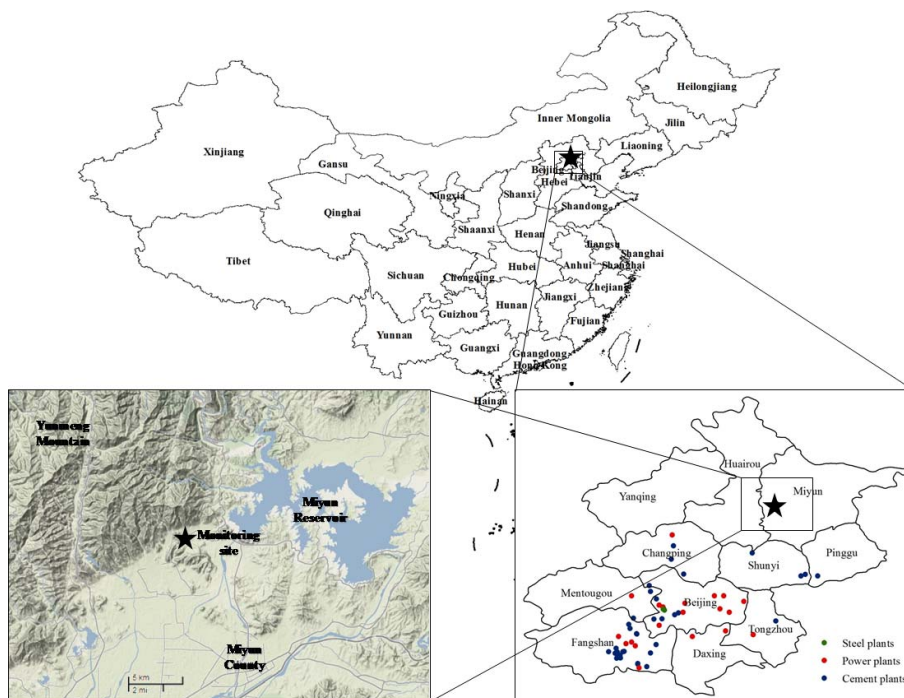


Fig. 1. The location of the Miyun monitoring station in Beijing, China. Notes: large point sources include power plants, cement plants, and iron and steel plants. Large power plants are defined as those whose installed capacities are larger than 6 MW. Large cement plants are defined as those whose production capacities of cement are larger than 15 ktyr^{-1} . Large iron and steel plants are defined as those whose production capacities of crude steel are larger than 1000 ktyr^{-1} .

[Title Page](#)
[Abstract](#)
[Introduction](#)
[Conclusions](#)
[References](#)
[Tables](#)
[Figures](#)
[Back](#)
[Close](#)
[Full Screen / Esc](#)
[Printer-friendly Version](#)
[Interactive Discussion](#)

Atmospheric mercury pollution in Beijing

L. Zhang et al.

Title Page

Abstract

Introduction

Conclusions

References

Tables

Figures

◀

▶

◀

▶

Back

Close

Full Screen / Esc

Printer-friendly Version

Interactive Discussion

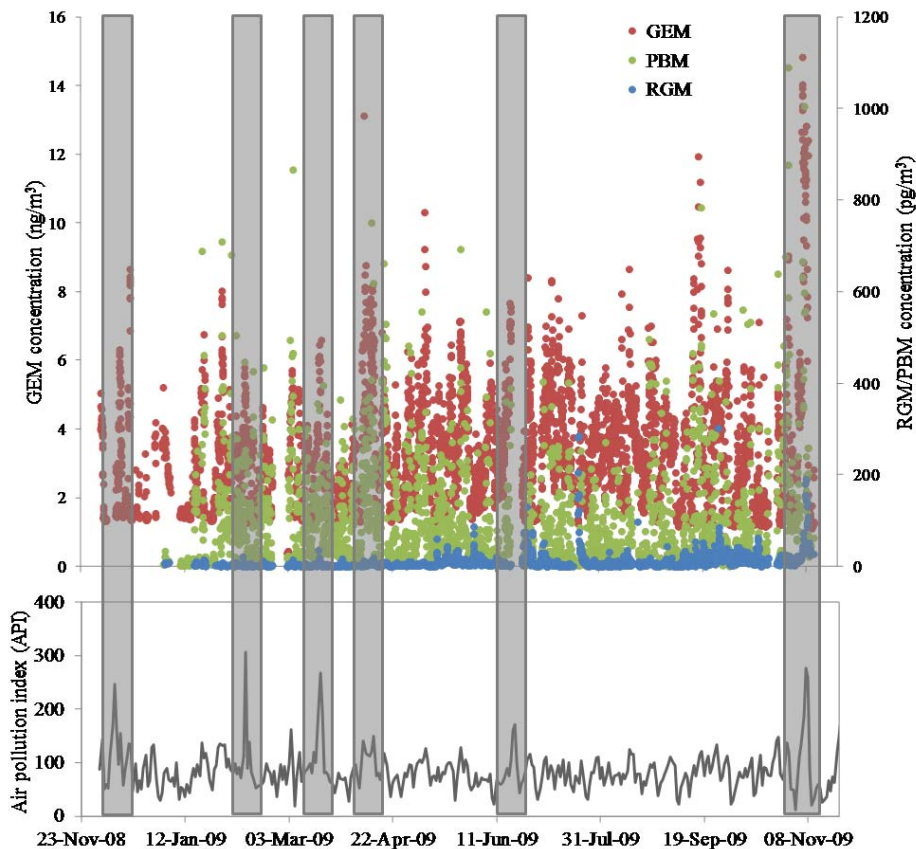


Fig. 2. Hourly averaged GEM, RGM and PBM concentrations at monitoring site and air pollution index (API) in Beijing urban area from December 2008 to November 2009. Notes: the six grey columns are typical heavy pollution episodes in Beijing urban area.

Atmospheric mercury pollution in Beijing

L. Zhang et al.

Title Page

Abstract

Introduction

Conclusions

References

Tables

Figures

◀

▶

◀

▶

Back

Close

Full Screen / Esc

Printer-friendly Version

Interactive Discussion

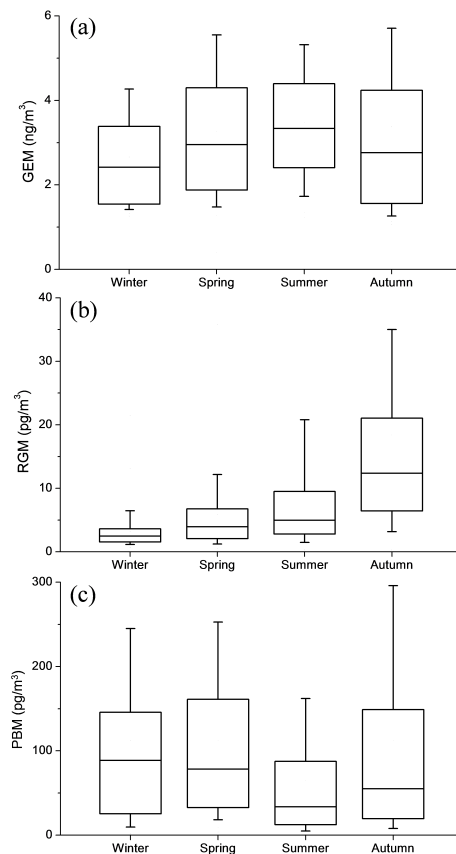


Fig. 3. Seasonal variation of **(a)** GEM, **(b)** RGM and **(c)** PBM concentration. Notes: the bottom and top of the box represent the 25th and 75th percentiles (the lower and upper quartiles), respectively. The band near the middle of the box represents the 50th percentile (the median). The ends of the whiskers represent the 10th and 90th percentiles.

Atmospheric mercury pollution in Beijing

L. Zhang et al.

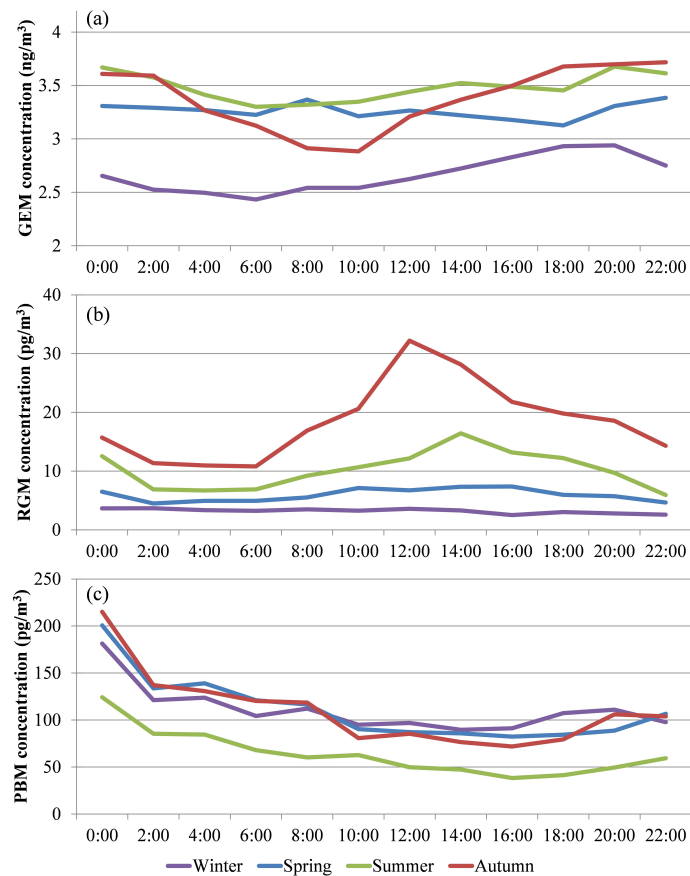


Fig. 4. Daily variation of **(a)** GEM, **(b)** RGM and **(c)** PBM concentration. Notes: the data was two hourly averaged.

Atmospheric mercury pollution in Beijing

L. Zhang et al.

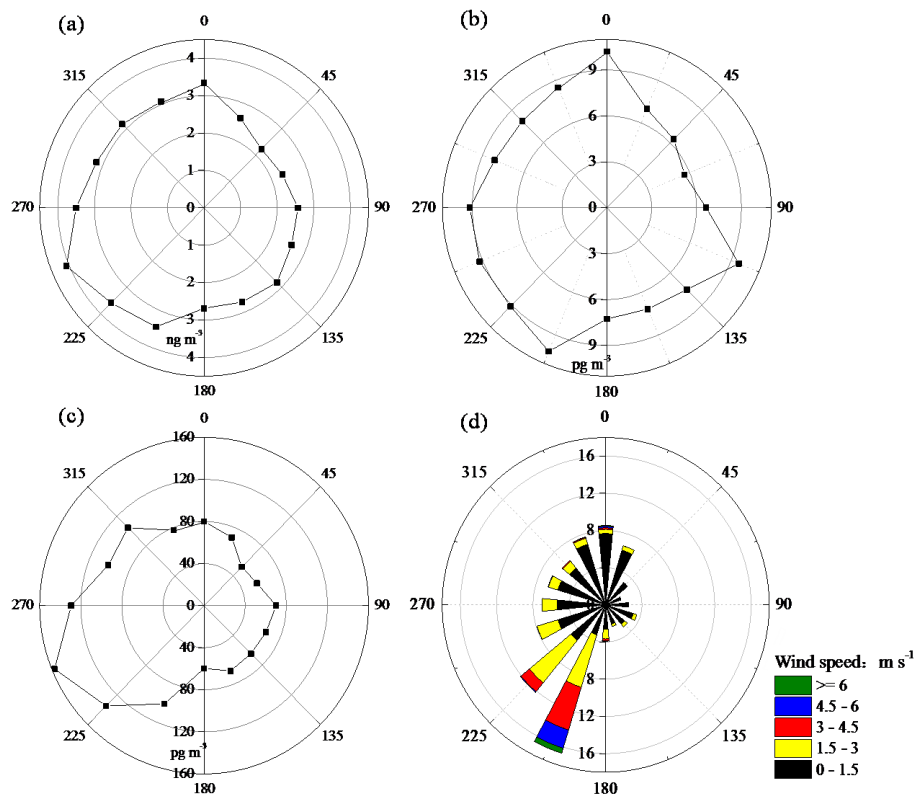


Fig. 5. Statistics of **(a)** average GEM concentration, **(b)** average RGM concentration, **(c)** average PBM concentration and **(d)** wind direction frequency in different wind directions.

[Title Page](#)
[Abstract](#)
[Introduction](#)
[Conclusions](#)
[References](#)
[Tables](#)
[Figures](#)
[Back](#)
[Close](#)
[Full Screen / Esc](#)
[Printer-friendly Version](#)
[Interactive Discussion](#)

Atmospheric mercury pollution in Beijing

L. Zhang et al.

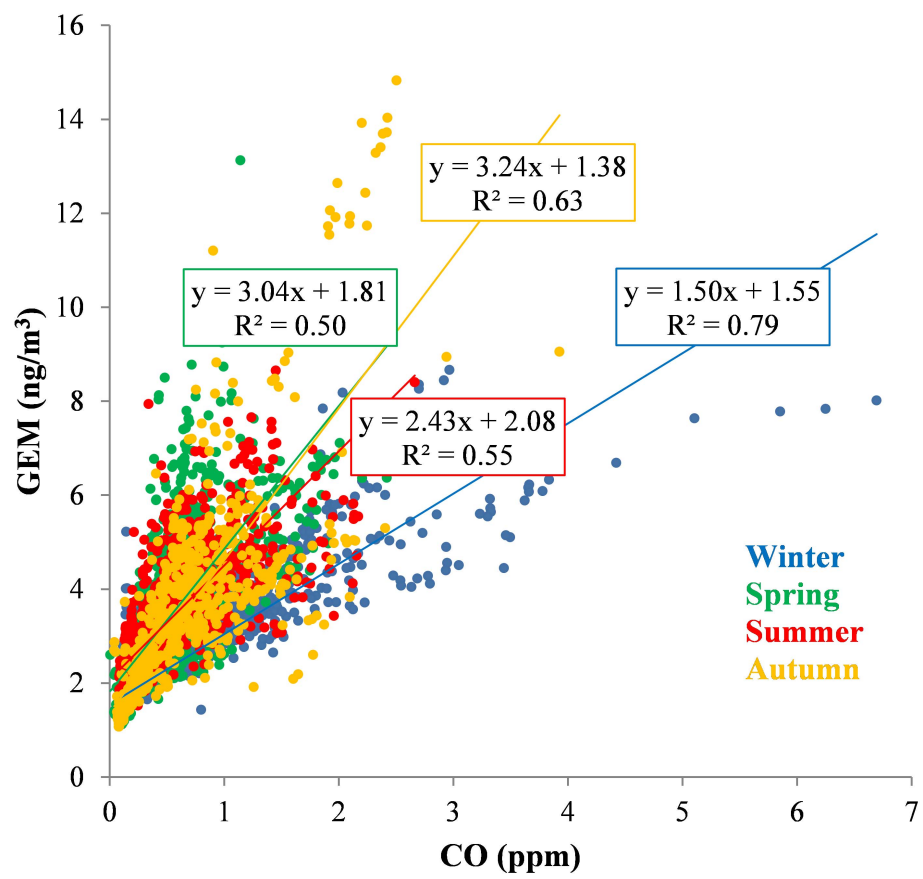


Fig. 6. Correlation between CO concentration and GEM concentration. Notes: the data was hourly averaged.

Title Page

Abstract Introduction

Conclusions References

Tables Figures

◀ ▶

◀ ▶

Back Close

Full Screen / Esc

Printer-friendly Version

Interactive Discussion



Atmospheric mercury pollution in Beijing

L. Zhang et al.

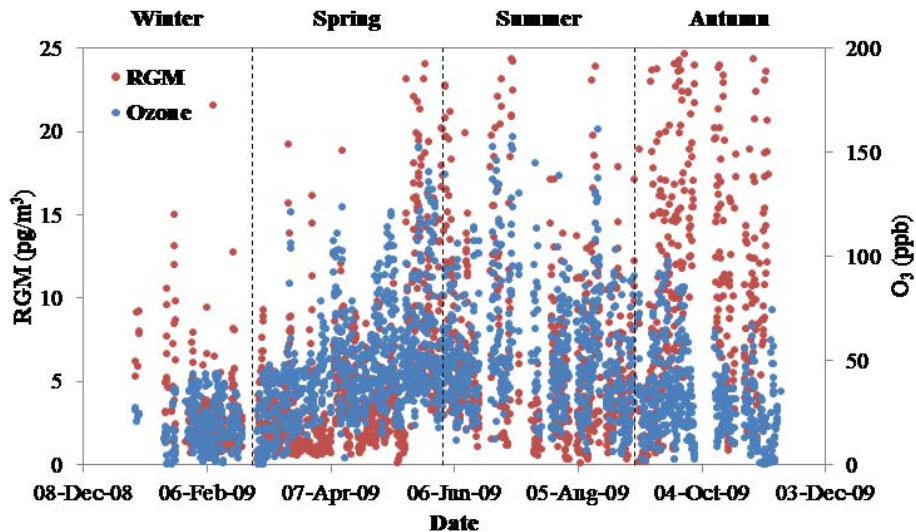


Fig. 7. Comparison of O₃ and RGM concentrations in different seasons. Notes: the data was hourly averaged.

[Title Page](#)[Abstract](#)[Introduction](#)[Conclusions](#)[References](#)[Tables](#)[Figures](#)[◀](#)[▶](#)[◀](#)[▶](#)[Back](#)[Close](#)[Full Screen / Esc](#)[Printer-friendly Version](#)[Interactive Discussion](#)

Atmospheric
mercury pollution in
Beijing

L. Zhang et al.

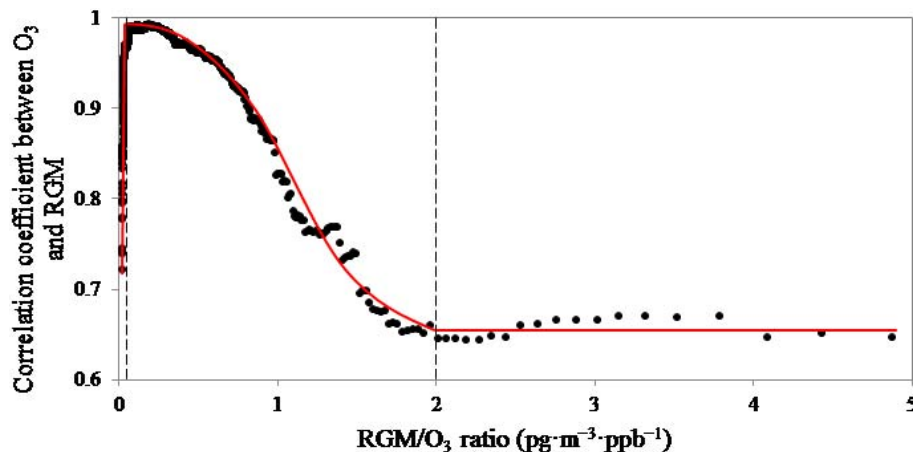


Fig. 8. Relationship between RGM/O₃ ratio and O₃-RGM correlation coefficient. Notes: the data was hourly averaged.

[Title Page](#)[Abstract](#)[Introduction](#)[Conclusions](#)[References](#)[Tables](#)[Figures](#)[◀](#)[▶](#)[◀](#)[▶](#)[Back](#)[Close](#)[Full Screen / Esc](#)[Printer-friendly Version](#)[Interactive Discussion](#)

Atmospheric
mercury pollution in
Beijing

L. Zhang et al.

Title Page

Abstract

Introduction

Conclusions

References

Tables

Figures

◀

▶

◀

▶

Back

Close

Full Screen / Esc

Printer-friendly Version

Interactive Discussion

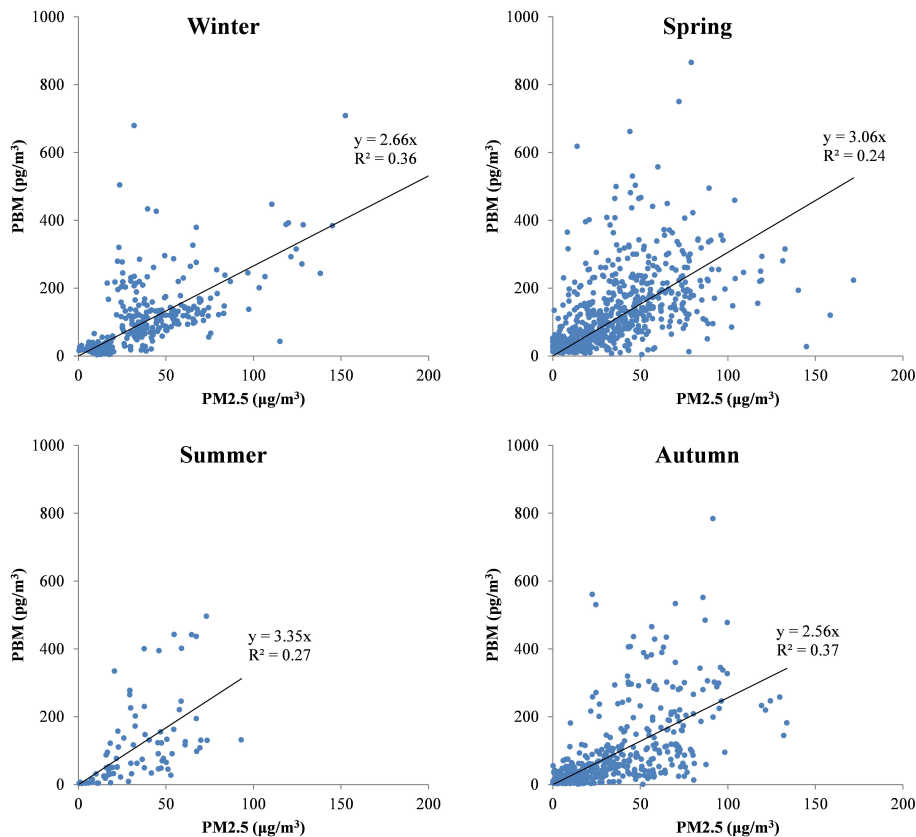


Fig. 9. Relationship between PM_{2.5} and PBM in different seasons. Notes: the data was hourly averaged.

Atmospheric mercury pollution in Beijing

L. Zhang et al.

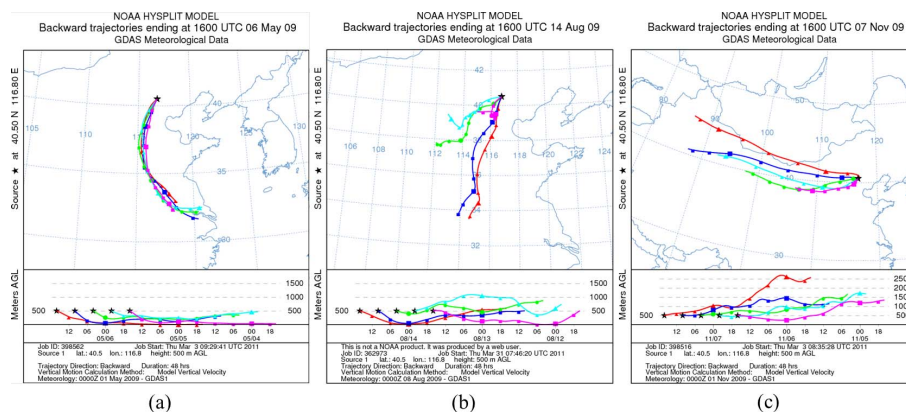


Fig. 10. HYSPLIT modeling results for the period of (a) 4–6 May, (b) 12–14 August, and (c) 5–7 November 2009.

Title Page

Abstract

Introduction

Conclusions

References

Tables

Figures

◀

▶

◀

▶

Back

Close

Full Screen / Esc

Printer-friendly Version

Interactive Discussion



Atmospheric
mercury pollution in
Beijing

L. Zhang et al.

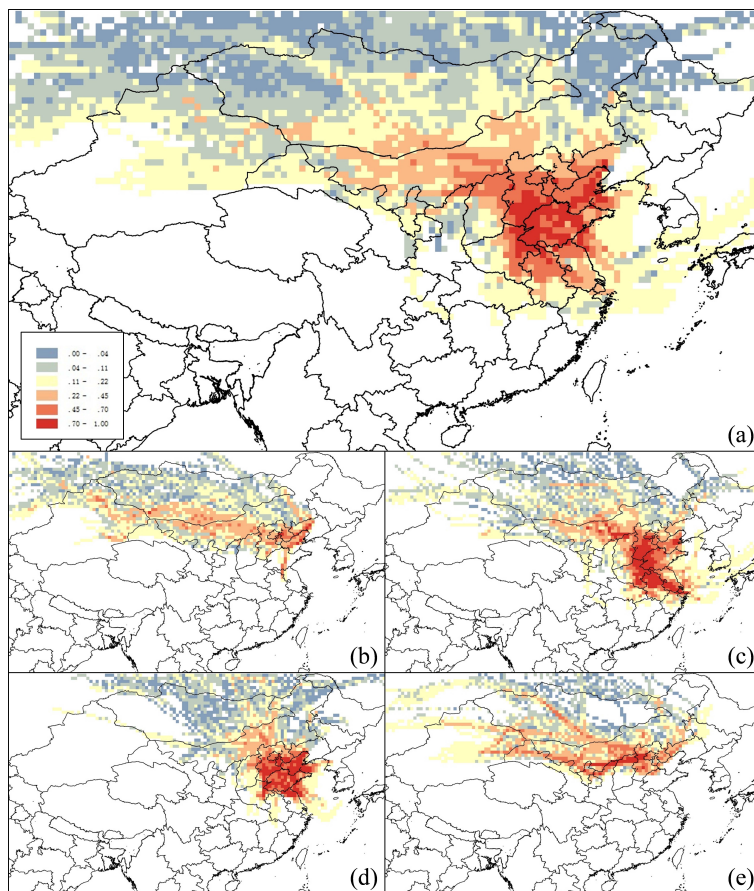


Fig. 11. Spatial contribution of mercury emission sources simulated by PSCF model (**a**: overall; **b**: winter; **c**: spring; **d**: summer; **e**: autumn).

[Title Page](#)[Abstract](#)[Introduction](#)[Conclusions](#)[References](#)[Tables](#)[Figures](#)[◀](#)[▶](#)[◀](#)[▶](#)[Back](#)[Close](#)[Full Screen / Esc](#)[Printer-friendly Version](#)[Interactive Discussion](#)